Interface ferromagnetism in a SrMnO_{3}/LaMnO_{3} superlattice

S. Smadici, B. B. Nelson-Cheeseman, A. Bhattacharya, and P. Abbamonte

Phys. Rev. B **86**, 174427 — Published 28 November 2012

DOI: 10.1103/PhysRevB.86.174427

INTERFACE FERROMAGNETISM IN A $SrMnO_3/LaMnO_3$ SUPERLATTICE

S. Smadici,[1] B.B. Nelson-Cheeseman,[2] A. Bhattacharya,[2,3] and P. Abbamonte[1]

[1] *Frederick Seitz Materials Research Laboratory, University of Illinois, Urbana, Illinois 61801*
[2] *Materials Science Division, Argonne National Laboratory, Argonne, Illinois 60439*
[3] *Center for Nanoscale Materials, Argonne National Laboratory, Argonne, Illinois 60439*

Resonant soft x-ray absorption measurements at the O K edge on a $SrMnO_3/LaMnO_3$ superlattice show a shoulder at the energy of doped holes, which corresponds to the main peak of resonant scattering from the modulation in the doped hole density. Scattering line shape at the Mn $L_{3,2}$ edges has a strong variation below the ferromagnetic transition temperature. This variation has a period equal to half the superlattice superperiod and follows the development of the ferromagnetic moment, pointing to a ferromagnetic phase developing at the interfaces. It occurs at the resonant energies for Mn^{3+} and Mn^{4+} valences. A model for these observations is presented, which includes a double-exchange two-site orbital and the variation with temperature of the hopping frequency t_{ij} between the two sites.

PACS numbers:

I. INTRODUCTION

Doped $La_{1-x}Sr_xMnO_3$ (LSMO) has multiple FM, AFM and canted magnetic orders as a function of doping and temperature[1–3] from superexchange[4] and double-exchange[5,6] interactions, which favor an antiferromagnetic (AFM) insulating phase and a ferromagnetic (FM) metallic phase, respectively. The FM phase at low temperatures is near the $x = 0.33$ doping, at which the closely related manganite $La_{1-x}Ca_xMnO_3$ shows very large ("colossal") magnetoresistance (CMR)[7].

The wave vectors of AFM and orbital orders in bulk manganites can be accessed with soft x-ray scattering at the Mn $L_{3,2}$ edges. For instance, studies were made for $Pr_{1-x}Ca_xMnO_3$ (Ref. 8), $La_{2-x}Sr_xMnO_4$ (Refs. 9–11) and $La_{2-2x}Sr_{1+2x}Mn_2O_7$ (Ref. 12) manganites. More recent measurements showed that magnetic and orbital scattering are similar in amplitude[13], studied the doping dependence[14], confirmed the separation in energy of Ref. 13 between the magnetic and orbital scattering resonances,[15] and studied their evolution after photoexcitation[16]. The broader features of the measurements are obtained in calculations of line shapes at the Mn $L_{3,2}$ edges with atomic multiplet models of magnetic[17] and orbital[18] scattering, and more recently, with a finite-difference method[19]. However, the investigation of the bulk FM phase near the $x = 0.33$ doping is not possible with soft x-ray scattering at the Mn L edges, due to lack of contrast for this order.

The FM phase can be studied with soft x-ray scattering in $(SMO)_n/(LMO)_{2n}$ superlattices (SL), in which the Sr and La atoms are ordered in $SrMnO_3$ (SMO) and $LaMnO_3$ (LMO) layers. External magnetic fields are not necessary, in contrast to x-ray magnetic dichroism experiments, where a reversible external magnetic field is applied to separate magnetic from charge x-ray scattering. The SL growth sequence can be used to define the period of a reflection along the c-axis and the symmetry of the structure. This was demonstrated for a $n = 4$ SL, in which the scattering wave vector was decreased to a range accessible at the O K edge resonance and interface scattering accessed with the high symmetry of the structure.[20]

In this work, we have applied these ideas to SL reflections at the O K and Mn $L_{3,2}$ edges and studied the development of the FM moment in a shorter superperiod $n = 2$ SL with soft x-ray absorption and scattering. Measurements at the O K edge showed modulated hole doping at oxygen sites. We have observed scattering at the Mn L edges from the SL interfaces at SL reflection $L = 2$, following the temperature dependence of the FM moment. The symmetry of the SL reflection allowed us to probe all Mn valences in the interface layers. In addition to Mn^{3+} valence resonances of bulk AFM order measurements[8–16], a peak in the resonant line shape, which has not been observed before, is aligned with the fluorescence yield edge for the Mn^{4+} valence. We present a model of the x-ray scattering from the SL interfaces, which includes the temperature dependence of the double-exchange hopping frequency t_{ij} and the change in the configurations of the Mn ions in the FM state.

II. EXPERIMENTS

A. Structure

The $n = 2$ SL was grown with molecular beam epitaxy on the (001) surface of $SrTiO_3$ (STO) at Argonne National Laboratory at 700 °C in a 2×10^{-6} Torr ozone pressure, followed by cooling to 100 °C and pump down. The structure was $\{r \times [2(SMO) + 4(LMO)] + SMO\}$ with $r = 13$ [Fig. 1(a)]. SMO ($a_{SMO} = 3.805$ Å, Ref. 21) and LMO ($a_{LMO} = 3.99$ Å, Ref. 22) layers on the STO substrate ($a_s = 3.905$ Å) are under +2.6 % tensile and −2.2 % compressive strain. The surface RMS roughness, measured with an atomic force microscope, was $\sigma_s = 2.85$ Å. From hard and soft x-ray reflectivity measurements, the SL superperiod was $c_{SL} = 22.5 \pm 0.5$ Å

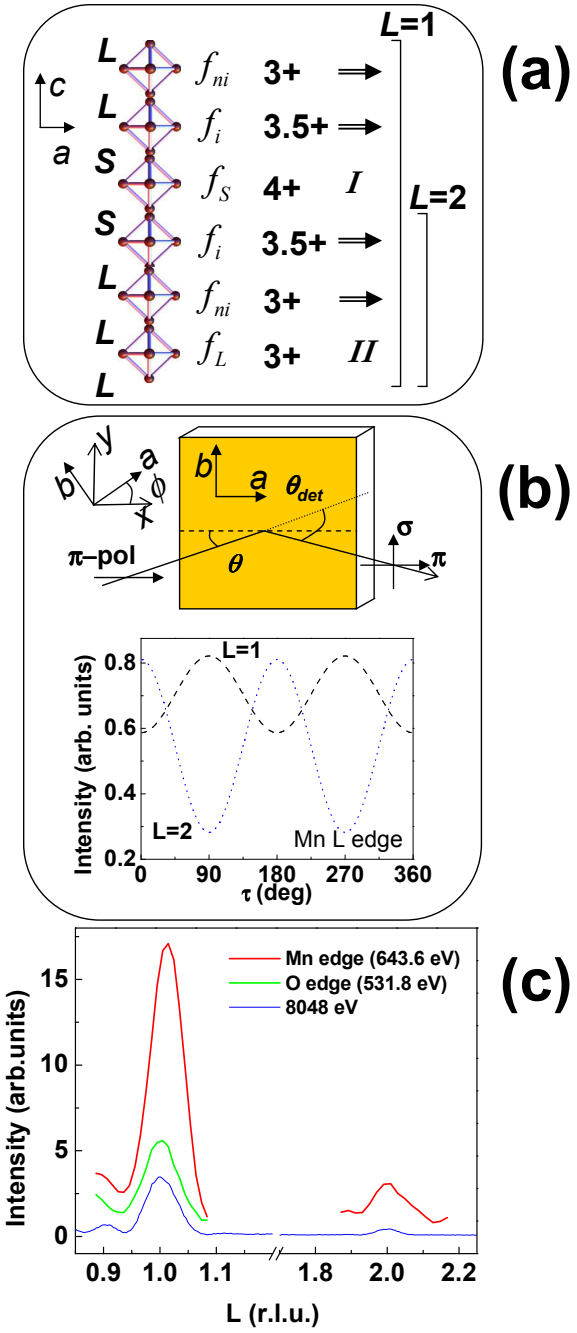

FIG. 1: (Color online) (a) Sketch of a 6 ML superperiod of the $(SMO)_2/(LMO)_4$ superlattice with LaO (L) and SrO (S) planes, layer form factors f, Mn valences in the MnO_2 planes estimated from the neighboring L or S planes, a magnetic order in the FM state and periods of the $L = 1$ and $L = 2$ SL reflections. SQUID hysteresis measurements with magnetic fields applied parallel and perpendicular to the SL surface showed that the magnetization easy axis is in-plane (data not shown). This confirms that the manganite layers were grown with the c-axis oriented along the normal to the surface and FM layers parallel to the surface. The spin direction in the SL surface plane was not known. (b) Scattering geometry for azimuth $\phi = 0°$, where ϕ is the angle made by the a-axis with the horizontal plane. The plot shows the calculated azimuthal dependence of magnetic scattering for angles θ and $\theta_{det} = 2\theta$, corresponding to the $L = 1$ and $L = 2$ reflections at the Mn L edge, where $\tau = \phi + \eta$ and η is the average magnetization angle with the tetragonal a-axis. (c) SL momentum scans at the Mn L_3, O K edges and with hard x-rays (8048 eV).

and the average c-axis parameter for 1 ML (a coverage of one formula unit of SMO or LMO over a $a_s \times b_s$ area) was 3.86 ± 0.05 Å.

B. X-ray absorption

X-ray absorption spectroscopy (XAS) measurements in fluorescence (FY) and electron yield (EY) modes were made at undulator beamline X1B at the National Synchrotron Light Source. The incident light was π-polarized and the incidence and detector angles were $\theta = 80°$ and $\theta_{det} = 110°$ [Fig. 1(b)]. The calculated energy resolution was 0.39 eV and 0.59 eV at O K (520 eV) and Mn L_3 (640 eV) edges, respectively.

SL FY and EY measurements at the O K edge show doped holes on the oxygen sites (Fig. 2). Because the probing depth exceeds the total SL thickness, FY has contributions from both the SL and the substrate. In contrast, because of the short electron escape depth, EY measurements are from the SL top layers only. The shoulder in FY measurements at 530.3 eV is aligned with the first peak in EY and is not present in FY measurements of the bare STO substrate. This shoulder corresponds to doped holes in LSMO (Ref. 24) and to the $L = 1$ scattering peak at 529.6 eV. The peak at 531.8 eV is from the STO substrate. The SL FY and EY measurements at the O K edge show no discernible variation with temperature between 300 K and 255 K.

SL FY and EY measurements at the Mn $L_{3,2}$ edges are compared to FY measurements on bulk samples with different Mn valences (Refs. 25–27) in Fig. 3. We removed the Mn^{2+} valence from further consideration because of the absence in the measured SL FY of the sharp peak at lower energies characteristic of Mn^{2+} FY (Fig. 3) and the expected Mn valences of a SMO/LMO superlattice (Mn^{4+} and Mn^{3+} for SMO and LMO layers, respectively). The SL FY measurement was aligned in energy with the average of bulk FY for the Mn^{3+} and Mn^{4+} valences, according to the number of SMO (Mn^{4+} valence) and LMO (Mn^{3+} valence) layers in one superperiod. No discernible variation was observed in FY or EY between 300 K and 255 K.

XAS measurements probe the average valence of O and Mn atoms in the SL. To discern a variation with temperature in different SL layers it is necessary to turn to scattering.

C. Resonant soft x-ray scattering

Resonant soft x-ray scattering (RSXS) measurements were made at the same beamline with an ultra-high vacuum diffractometer. For other RSXS experiments on bulk and SL at this endstation see Refs. 20,23,28–31. The incident beam was π-polarized and the measurement integrated both π and σ scattering channels. The

scattering momentum $Q = (0, 0, 2\pi L/c_{SL})$ in the reflectivity geometry with $\theta_{det} = 2\theta$ is indexed with respect to the SL superperiod c_{SL}. The energy resolution was 0.20 eV and 0.34 eV at O K (520 eV) and Mn L_3 (640 eV) edges, respectively. The different energy resolutions of XAS and RSXS measurements originate from different slit settings which, in order to protect the channeltron detector, were more closed in the specular RSXS scattering geometry. The relative alignment of XAS and RSXS spectra at the resonant edges was determined from two measurements with the corresponding slit settings and scattering geometries, taken a few minutes apart. The sample was cooled in zero magnetic field and scattering measurements for $L = 1$ at the O K edge and for $L = 1, 2$ at the Mn $L_{3,2}$ edges [Fig. 1(c)] were made at different temperatures (Figs. 2 and 4).

FM order in metallic films has been studied with x-ray resonant magnetic scattering of linearly[32] and circularly[33] polarized light at the Fe and Co L edges, with an external magnetic field applied to separate the magnetic from charge scattering. The FM order in a Ag/Ni SL has been investigated with circularly polarized light[34]. However, unlike previous studies, the SL FM order is accessed here at SL reflections with no applied magnetic fields and with linearly polarized light.

1. *O K edge line shape*

The spatial modulation in the density of holes doped on the oxygen sites can be observed with RSXS. Specifically, the O K edge line shape for $L = 1$ scattering shows a peak close to the energy of the shoulder in FY measurements (Fig. 2).

Since the order of levels in the RSXS line shape at the O K edge follows that of the ground state, the RSXS line shape can be analyzed using the hybridization between O p and Mn e_g levels in the ground state. Fig. 2 (inset) shows the unoccupied $e_{g,\uparrow}$, $t_{2g,\downarrow}$ and $e_{g,\downarrow}$ levels in SMO. XAS experiments and calculations at the Mn L edge (Ref. 35) give a crystal field splitting $10Dq$ between the e_g and t_{2g} levels of 2.4 eV for bulk SMO and 1.5 eV for LMO. The scattering line shape at the O edge is described well by O p states hybrids with the Mn e_g levels in the SMO and LMO layers, shown with arrows in Fig. 2, followed at higher energy by hybrids with La and Sr states. Two $e_{g,\downarrow}$ levels (3.5 eV and 5 eV above $e_{g,\uparrow}$) are present in LMO and only one for SMO (3.5 eV above $e_{g,\uparrow}$) (Ref. 36) because the electron in the $e_{g,\uparrow}$ level in LMO splits the unoccupied $e_{g,\downarrow}$ levels by Coulomb interaction, even in the absence of any Jahn-Teller distortion.

However, no variation across the FM transition is observed within the error bars. To access T-dependent interface states (Sec. III A), it is necessary to reach the $L = 2$ reflection, for which the O K edge energy is too low. In contrast, $L = 2$ is accessible at the Mn $L_{3,2}$ edges.

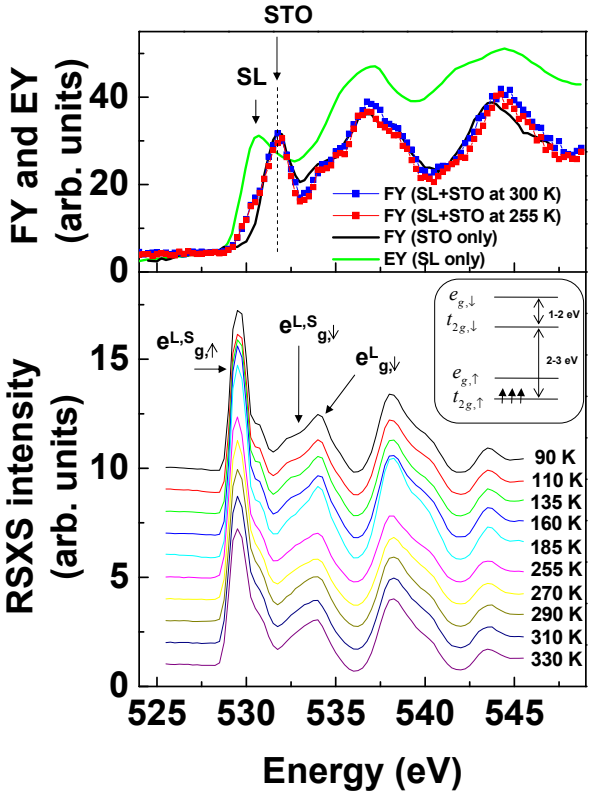

FIG. 2: (Color online) Top: FY at the O K edge for the SL on STO at different temperatures and the bare STO substrate (black line), compared to EY measurements. FY measurements were aligned with the linear transformation $FY_{plotted} = aFY_{measured} + b$, where a and b are constants. Bottom: Temperature dependence of resonant scattering at $L = 1$. The scans have been normalized to the pre-edge values and shifted vertically for clarity. The inset shows the order of the energy levels for SMO in the ground state, with the Jahn-Teller splitting neglected. LMO has an additional electron in the $e_{g,\uparrow}$ level and a split upper level $e_{g,\downarrow}$.

2. *Mn $L_{3,2}$ edge valences*

There is no discernible variation in the line shape at $L = 1$ at the Mn $L_{3,2}$ edges across the FM transition temperature (Fig. 4). However, a pronounced variation is visible for $L = 2$. From under the relatively broad XAS at the Mn L edge, T-dependent RSXS at $L = 2$ selects those states that are sensitive to the temperature variation. Specifically, an increased intensity of the A, B and C peaks at lower T, and a decreased intensity of the α peak is observed at the L_3 edge (Fig. 4). Parallel variations occur at the L_2 edge for peaks E, F and β. Two-dimensional maps of the scattering intensity in L and E variables are shown in Fig. 5, to place the cuts in L in Fig. 1(c) and E in Fig. 4 in the context of the overall measurement. The temperature dependence of height and width of peak C are shown in Fig. 6.

The magnetic scattering dependence on the unknown in-plane spin orientation raises the question of variations

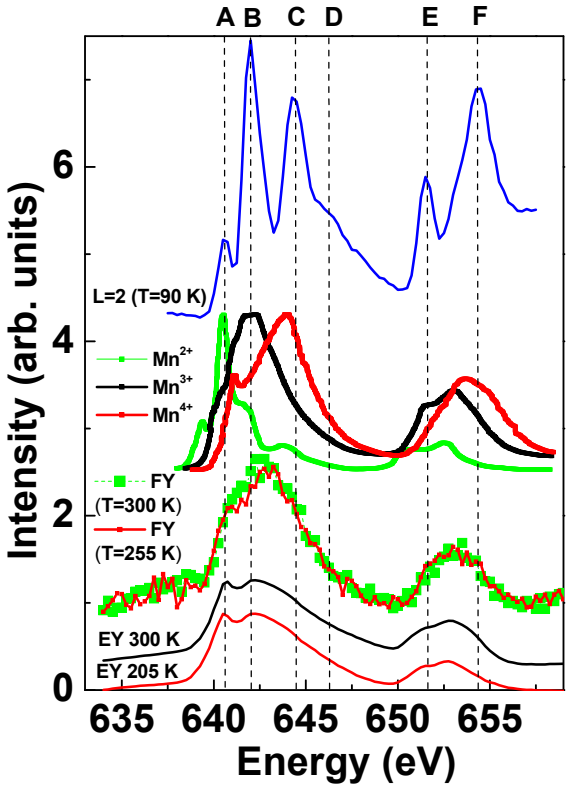

FIG. 3: (Color online) SL EY and FY (lower curves) and RSXS (top) at $L = 2$ at the Mn $L_{3,2}$ edges compared to FY measurements for different Mn valences (middle, all from Ref. 26). All three Mn valences were measured in each of Refs. 25–27. For clarity, only the measurements from Ref. 26 are shown.

in the line shape with the azimuthal angle ϕ between the a-axis and the horizontal plane. We calculated the dependence of the magnetic scattering intensity on $\tau = \phi + \eta$, where η is the unknown average magnetization angle with the tetragonal a-axis, for incident angles θ corresponding to the $L = 1$ and $L = 2$ reflections at the Mn L edge and detection integrating over both π and σ final state polarizations. The intensity variation in arbitrary units is between ∼0.6 and 0.8 for $L = 1$ ($\theta \sim 25°$) and between ∼0.3 and 0.8 for $L = 2$ ($\theta \sim 60°$) [Fig. 1(b)]. A complete cancelation of the magnetic scattering intensity can be ruled out. This is confirmed by temperature-dependent measurements for azimuthal angles along the tetragonal ($\phi = 0°$) and orthorhombic ($\phi = 45°$) directions at $L = 1$ (only $\phi = 0°$ data shown in Fig. 4) and $L = 2$ (Figs. 4 and 5 for $\phi = 0°$ and $\phi = 45°$, respectively). The line shape at $L = 2$ showed the same peaks (A to F, α and β) for both azimuthal angles ϕ, consistent with the azimuthal dependence of magnetic scattering.

Coulomb and exchange interactions for ground and RSXS excited states are different at the Mn $L_{3,2}$ edges. An analysis of the RSXS line shapes based on ground state calculations, similar to that at the O K edge, cannot be made. However, both FY and RSXS measurements probe excited states and FY measurements on bulk samples for different Mn valences (Fig. 3, middle) will be used to identify the valence of scatterers for different resonances in the RSXS line shapes. This approach is supported by the relatively small difference in energy between RSXS resonances for scatterers of the same valence and different specific scattering contrasts ($\lesssim 1$ eV between magnetic and orbital scattering for bulk measurements[13,15]) compared to the ~ 2 eV separation in energy between the main FY features for different valences.

In general, the energy alignment between FY (from the imaginary part) and RSXS (from both real and imaginary parts) resonances of a scattering state is expected to be correct up to a difference on the order of the intrinsic linewidth. In our particular case, the main features in FY at the Mn L_3 edge for the three different Mn valences are fortuitously separated by ~ 2 eV (Fig. 3), which is larger than the measured linewidth [~ 1 eV in Fig. 6(b)] and the intrinsic linewidth. Specifically, peak C in scattering at $L = 2$ (blue line in Fig. 3) is close in energy to the main peak of the Mn^{4+} valence (the small difference may be attributed to the mentioned limits of FY and RSXS peak alignment) and coincidentally far (> 2 eV) from the main features in FY of the Mn^{3+} or Mn^{2+} valences.

In addition, the correspondence of peak C to scattering from Mn^{4+} ions explains the absence of this peak in all RSXS measurements on bulk manganites. Specifically, measurements on bulk 113 (Ref. 8), 214 (Ref. 9–11) and 327 (Ref. 12) manganites in the AFM state observe two main resonances at the Mn L_3 edge, at A and B only. The in-plane distribution of the Mn^{4+} ions has a spatial periodicity of 2 u.c. (Refs. 8,9). Therefore, scattering from Mn^{4+} ions is not allowed at the in-plane 4 u.c. reflection wave vector along the tetragonal axes.

FY measurements in Sec. II B showed that the Mn^{2+} valence is absent in the SL. The A and B resonances in the RSXS line shape for $L = 2$ correspond to the Mn^{3+} valence since they are observed in measurements on bulk manganites, while resonance C lines up at the energy of FY edge for the Mn^{4+} valence. More T-dependent measurements on SL with different superperiods are needed before a discussion of peak α. It is clear that a more detailed model is needed to quantitatively model the entire line shape at the Mn L_3 edge. We limit our discussion in Sec. III B to peak C.

III. DISCUSSION

The model of Sec. III A relates the absence of variation with temperature in the scattering contrast for $L = 1$ and the variation for $L = 2$ to changes in the form factor δf_i of interface layers and interface ferromagnetism.

The line shape variation with the transition from the PM to the FM state for specific interface magnetic and

orbital x-ray scattering models is discussed in Sec. III B.

A. Interface ferromagnetism

The scattering intensity $I \propto \left|S + \delta S\right|^2$ follows the evolution with temperature of the FM moment [Fig. 6(a)]. The line shape and structure factor at the Mn edge at $L = 2$ (Fig. 4) are made of two parts. The T-independent structure factor $S(Q) = \sum_l f_l e^{iQz_l}$ is given by the SL structure, to which a T-dependent contribution δS is added with the transition to the FM state.

The absence of a variation with temperature in the scattering intensity at $L = 1$ [$\delta S(L = 1) = 0$] and the variation at $L = 2$ [$\delta S(L = 2) \neq 0$] strongly suggests that the unit cell of the T-dependent contribution to the structure factor δS is half the SL superperiod or 3 ML (higher momenta L are not accessible at the Mn L edges). The middle of the SMO and LMO layers (separated by 3 ML) are the most dissimilar parts of the SL structure, while the SMO/LMO and LMO/SMO interfaces (with two interfaces every superperiod, also separated by 3 ML) are similar. In the following, we consider a scattering component δS that develops at the SL interfaces.

These conditions are contrary to those expected for scattering contrast from crystal field effects or structural differences in a SL, from either differences in the c-axis lattice constants or Jahn-Teller distortions, which do not have a 3 ML unit cell. In addition, no discernible variation was observed for scattering at the La $M_{5,4}$ edges for $L = 1$ or $L = 2$ between 300 K and 225 K (data not shown). This shows that the change δS is due to a variation with temperature in the resonant form factors of the SL layers (δf_l), not of structural factors (δz_l).

The possibility that the transition to the FM state gives exclusively non-magnetic scattering contrast is not supported by an analysis of the line shape variation with temperature (Sec. III B). The T-dependent scattering δS is, at least partially, magnetic in origin and, for simplicity, we discuss only x-ray resonant magnetic scattering in this section. Orbital contributions to δS are addressed in Sec. III B.

The scattering form factors $(f)^{mn}$ and $(\delta f)^{mn}$ are tensors, which are multiplied with the final ($\hat{\epsilon}_f$) and initial ($\hat{\epsilon}_i$) light polarization vectors. This gives an overall factor which, for charge (S) and magnetic (δS) scattering, is

$$S \propto \hat{\epsilon}^*_{f,m}(f)^{mn}\hat{\epsilon}_{i,n} \propto (\hat{\epsilon}^*_f\hat{\epsilon}_i)\, f(\omega) \quad (1)$$

$$\delta S \propto \hat{\epsilon}^*_{f,m}(\delta f)^{mn}\hat{\epsilon}_{i,n} \propto i[(\hat{\epsilon}^*_f \times \hat{\epsilon}_i)\hat{z}_l]\, \delta f(\omega) \quad (2)$$

where $\hat{z}_l$ is the direction of the local moment at site l (Refs. 32,34). The sum over the in-plane sites l for each layer is proportional to the magnetization $\overrightarrow{M}$ of the layer. $f(\omega)$ and $\delta f(\omega)$ are scalar functions.

The scattering contrast of the RSXS peaks that persist above the FM transition temperature, held constant by

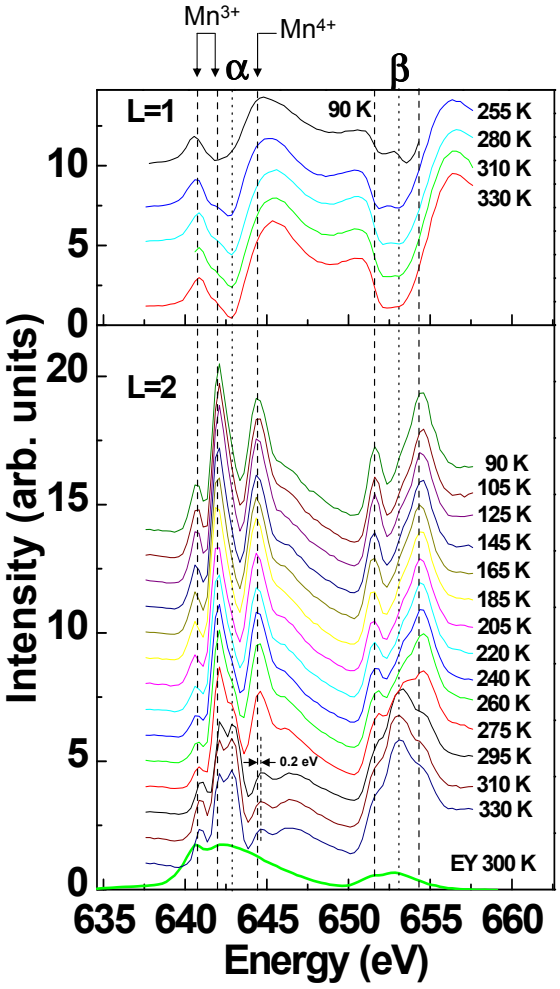

FIG. 4: (Color online) Temperature dependence of RSXS at the Mn $L_{3,2}$ edges at $L = 1$ and $L = 2$ for azimuthal angle $\phi = 0°$.

the internal field between Sr^{2+} and La^{3+} ions arranged in the SL layers, is defined by the SL structure. With the form factors shown Fig. 1(a) for "interface" (f_i), "near-interface" (f_{ni}), "middle SMO" (f_S) and "middle LMO" (f_L) layers, and neglecting inter-diffusion roughness and structural differences between SMO/LMO and LMO/SMO interfaces, the T-independent structure factors S at $L = 1, 2$ are

$$S(L = 1) = -f_L + f_S + f_i - f_{ni} \quad (3)$$

$$S(L = 2) = f_L + f_S - f_i - f_{ni} \quad (4)$$

The origin has been chosen so that an arbitrary phase factor between $S(L = 1)$ and $S(L = 2)$ is zero.

The 3 ML unit cell of T-dependent scattering sets more stringent constraints on the variation of δf_l in the SL, beyond the experimental observation $\delta S(L = 1) = -\delta f_L + \delta f_S + \delta f_i - \delta f_{ni} = 0$. To obtain a 3 ML unit cell, the variation in the interface and near-interface layers must be equal, $\delta f_i = \delta f_{ni}$. Similarly, the measurements imply that two regions within a superperiod scatter dif-

ferently from the FM i and ni layers and that the T-dependent scattering in these two regions is the same. With one the middle of the SMO layers the other must be the middle of the LMO layers, or $\delta f_S = \delta f_L$.

FM order in the i and ni layers with $(\delta f_i)_{\rm mag} = (\delta f_{ni})_{\rm mag}$ is consistent with estimates of the average Mn valence in a MnO_2 plane based on the type (L or S) of neighboring planes [Fig. 1(a)]. Specifically, a comparison to magnetic orders of equivalent bulk LSMO doping shows that Mn^{3+} and $Mn^{3.5+}$ valences are near the FM dome for bulk LSMO. The magnitude of the FM moment depends on the Mn valence and implicitly on the SL interface roughness, with structural imperfections in a $(SMO)_{4.4}/(LMO)_{11.8}$ SL correlating with the average interface FM moment.[38] However, the FM moment distribution is more symmetrical in the smaller superperiod $n = 3$ SL (Ref. 39), consistent with the symmetric FM moment distribution in Fig. 1(a).

Since $(\delta f_S)_{\rm mag} = (\delta f_L)_{\rm mag}$, the f_S and f_L layers have either the same magnetization $\overrightarrow{M}$ or no magnetization at low temperatures. The different hole doping of these layers does not support the possibility of an equal magnetization. The remaining possibility is that, as the SL is cooled and becomes FM in zero applied field, there is no magnetization in both these layers, or $(\delta f_S)_{\rm mag} = (\delta f_L)_{\rm mag} = 0$. Therefore, the FM phase is localized at the SL interfaces.

A model of the FM state for a SL superperiod is shown in Fig. 1(a), where I and II represent magnetic phases of the f_S and f_L layers, with an average zero magnetization in no applied fields (in contrast, the polarized neutron reflectivity measurements in Refs. 38,41 were made in applied fields). There are several different possible I and II phases with no net magnetization: a PM phase, an ordered AFM phase (for instance, a C-type or a G-type near the Mn^{4+} doping of bulk LSMO and f_S layers), or an irregular phase with canted moments[41] pointing in different directions in the sample regions with slight variations in local doping[3] (near the the Mn^{3+} doping of f_L layers).

PM I or II phases, at least for the higher temperature range, below the SL FM transition temperature of 305 K [Fig. 6(a)], are suggested by the valences of the f_S and f_L layers, which are close to Mn^{4+} and Mn^{3+}. These correspond to G-type and A-type AFM magnetic orders in bulk SMO and LMO, with transition temperatures of $T_{N,SMO} = 235$ K (Ref. 21) and $T_{N,LMO} = 135$ K (Ref. 37), respectively. However, the SL saturation FM moment of $\sim 2.5\ \mu_B$ at 5 K (Ref. 40) gives an extent along the c-axis of the FM region in high fields of $\gtrsim (2.5/3.22)\times 6$ ML ~ 4.65 ML for each superperiod, where $\sim 3.22\ \mu_B$ is the maximum FM moment of the $x = 0.33$ alloy[39]. This value is too high for both f_S and f_L layers to remain PM at the lowest temperatures. Therefore, at least one other magnetic transition occurs in the f_S or f_L layers from a PM phase at higher temperatures to a different phase at lower temperatures. However, in contrast to the FM transition in the i and ni layers, the magnetic RSXS

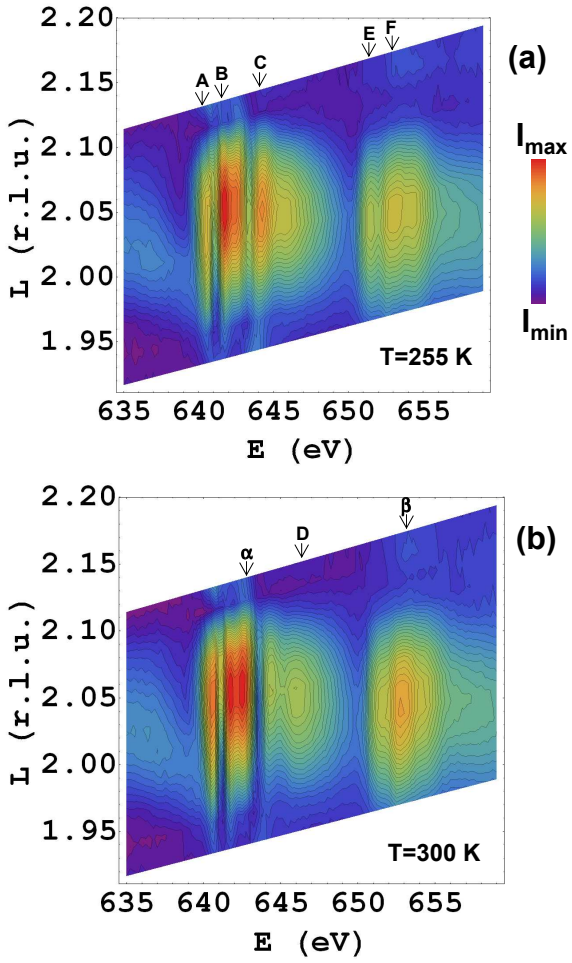

FIG. 5: (Color online) Two-dimensional resonance profiles at the Mn $L_{3,2}$ edges at 255 K and 300 K for azimuth $\phi = 45°$.

intensity would not vary at these transitions if there is no average layer magnetization in the low temperature phases.

With the constraints on δf_l, the change in the structure factor $\delta S(Q) = \sum_l \delta f_l e^{iQz_l}$ for the FM transition and $L = 1, 2$ from Eqs. (3)-(4) is

$$\delta S(L = 1) = 0 \quad (5)$$

$$\delta S(L = 2) = -2\delta f_i \quad (6)$$

where $\delta f_i = f_{i,\rm FM} - f_{i,\rm PM} = \delta f_{ni}$. Eq. (6) relates the changes with temperature in the line shape at $L = 2$ to variations in the form factor of interface and near-interface layers with the transition to the FM state.

The $\delta S(L = 2)$ reflection is allowed in this $n = 2$ SL for all Mn sites in the FM layers. However, scattering from a Mn^{4+} valence was not observed at $L = 3$ for a $n = 4$ SL (Ref. 20) [it was observed at $L = 3$ for a $n = 3$ SL (data not shown)]. The symmetry that very effectively forbids reflections from the Mn^{4+} ions at $L = 3$ for a $n = 4$ SL is not known and surprising, given inherent small imperfections of a SL structure. More measurements are needed on different SL to answer this question.

B. Interface x-ray scattering

We now discuss the temperature variation of the RSXS line shape at $L = 2$ and Mn $L_{3,2}$ edges.

The width of resonance C, corresponding to scattering from Mn^{4+} ions in the interface and near-interface layers, has a sharp increase at the FM transition temperature [Fig. 6(b)]. The increase in the scattering intensity in the FM state is also taking place ~ 0.2 eV below the x-ray charge scattering resonance [from diagonal terms of the scattering factor f in Eq. (1)], that corresponds to the Mn^{4+} valence in the PM state (at 644.65 eV in Fig. 4).

In general, the line shape of resonant magnetic scattering is related to variations in the occupation of orbitals induced by a magnetic field[42] near the absorption edges for Mn ions of different (Mn^{3+} and Mn^{4+}) valences. However, the magnetic scattering is slightly shifted to lower energies compared to orbital scattering for AFM bulk orders.[13,15] We cannot resolve two peaks at C in the SL line shapes at low T, but this suggests that, with the increase of the FM moment at lower T, a T-dependent magnetic scattering contribution is added ~ 0.2 eV below the charge scattering resonance. This addition to f_i of a temperature dependent $(\delta f_i)_{\rm mag}$ explains the observed variation in line shape at $L = 2$. The charge scattering resonance might also increase at lower T, concomitantly with magnetic scattering and variations in orbital scattering with T are discussed briefly at the end of this Section.

A more gradual increase in width is observed at lower T [Fig. 6(b)]. For x-ray scattering in the FM phase, it is necessary to consider a double-exchange two-site orbital, which suggests that this width increase is related to the T dependence of the double-exchange frequency t_{ij} between the two Mn sites. Both resonant magnetic and orbital scattering are ultimately scattering off orbitals, and the consideration of two-site orbitals in the FM state applies to both cases.

The double-exchange process involves two coordinated jumps from the Mn to the O atoms [Fig. 6(b), inset]. It is useful to consider the simpler process of one jump first, which is sometimes included in XAS calculations of complex oxides. In this case, inter-site charge transfer between d-states of a transition metal and a neighboring (ligand, L) O ion[43] and consideration of multiple configurations (for instance, d^8 and $d^9\underline{L}$ for Cu^{1+} and Cu^{2+} valences) change the scattering form factor f at the transition metal edge. In particular, satellite peaks develop in XAS (and, implicitly, in RSXS) at additional Cu valences.[44]

In the double-exchange process, specific to FM complex oxides, charge transfer takes place between transition metal sites, beyond the neighboring O atoms. Specifically, the $|\psi_1\rangle$ and $|\psi_2\rangle$ configurations are coupled in a two-site ground state wave function [Fig. 6(b), inset],

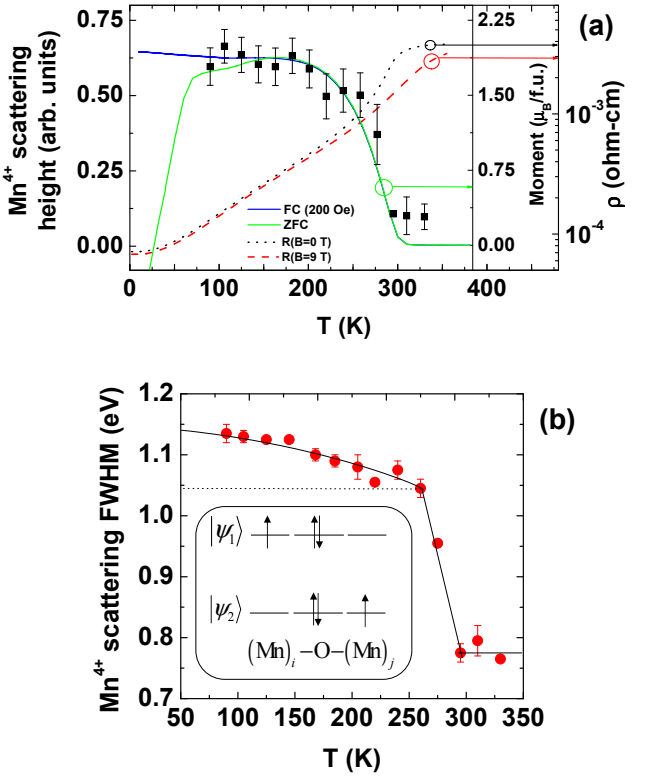

FIG. 6: (Color online) (a) Temperature dependence of resonance C height for $\phi = 0^\circ$ compared to the SL FM moment measured with SQUID for ZFC and in-plane FC=200 Oe (Ref. 40). The SL has a 305 ± 5 K FM transition temperature, which is lower than the ~ 355 K transition temperature of the $x = 0.33$ LSMO alloy (Ref. 39). SL resistivity becomes metallic-like at low T (Ref. 40). (b) Temperature dependence of resonance C width. The line is a guide to the eye. Inset shows a sketch of the double-exchange configurations $|\psi_1\rangle$ and $|\psi_2\rangle$ for Mn sites i and j (Ref. 5).

which for this FM manganite is

$$|\psi_\pm\rangle = \frac{1}{\sqrt{2}}(|\psi_1\rangle \pm |\psi_2\rangle) \qquad (7)$$
$$|\psi_1\rangle = |\mathrm{Mn^{3+}}, \mathrm{O^{2-}}, \mathrm{Mn^{4+}}\rangle$$
$$|\psi_2\rangle = |\mathrm{Mn^{4+}}, \mathrm{O^{2-}}, \mathrm{Mn^{3+}}\rangle$$

with Mn valences in FM layers in a superposition of Mn^{3+} and Mn^{4+}. In the ground state (without an x-ray photon absorbed), the charge transfer splits the two levels $|\psi_\pm\rangle$ by the exchange energy $2t_{ij}$ (Ref. 5), where the double-exchange hopping between sites i and j is $t_{ij} = t_{\rm DE}\cos[(\theta_{\rm i} - \theta_{\rm j})/2]$, with $t_{\rm DE}$ a constant and $\theta_{i,j}$ the $t_{2g,\uparrow}$ spins orientations on the two sites (Ref. 6). More precisely, the bandwidth of e_g electrons in the ground state depends on the hopping frequency between the i and j sites as[37]

$$W \propto \cos[(\theta_{\rm i} - \theta_{\rm j})/2]\cos\phi \propto t_{ij}\cos\phi \qquad (8)$$

where $(\pi - \phi)$ is the angle between the Mn-O-Mn bonds.

To account for the double-exchange process in x-ray scattering, the orbitals $|\psi_{1,2}\rangle$ are replaced with the two-site orbitals $|\psi_{\pm}\rangle$. Similar to the case of satellite peaks for ligand holes on oxygen atoms, the charge transfer between Mn sites beyond the neighboring O atoms changes the scattering factor f at peaks in RSXS, which correspond to the Mn^{3+} and Mn^{4+} valences. In addition, the splitting by $2t_{ij}$ of the $|\psi_{\pm}\rangle$ states or the bandwidth W of e_g electrons in the ground state are transferred to an increased measured RSXS line width.

The hopping frequency t_{ij} increases with increased FM order of spins $\theta_{\mathrm{i,j}}$ at lower T, and broadens the scattering form factors f and the line width. In this model, the XAS and therefore, the RSXS peaks, should become broader at lower temperatures. The width increase at lower temperatures of peak C [Fig. 6(b)] is consistent with this model and $t_{\mathrm{band}} \sim 0.2 - 0.5$ eV for each of the e_g states, $2t_{\mathrm{DE}} \sim 2T_{\mathrm{Curie}} \sim 0.05$ eV and contributions from experimental resolution (0.34 eV at the Mn L edge) and core-hole width ($w_{\mathrm{FWHM}} \sim 0.3 - 0.5$ eV, Ref. 8).

In addition to the double-exchange processes in the FM state, lattice distortions are also relevant to the CMR transition[45,46]. In bulk manganites, they may depend on T, changing the bond alignment angle ϕ and bandwidth W [Eq. (8)]. However, the average angle between the Mn-O-Mn bonds for SL samples is fixed by the substrate.

Orbital scattering at the Mn L edges has a comparable amplitude to magnetic scattering for bulk AFM orders.[13,15] It can come from occupation contrast or polarization contrast from different atomic orbital orientations in the anomalous scattering tensor. The analogous occupation contrast in SL FM is a T-dependent charge transfer across SL interfaces (which includes the electronic reconstruction of Ref. 20), in addition to the T-independent part defined by the SL structure. The T-dependent polarization contrast in the SL may also be substantial; for instance, on closely related SL (Ref. 47), in-plane $e_g(x^2 - y^2)$ occupation and FM near LMO interfaces and out-of-plane $e_g(3z^2 - r^2)$ orbital occupation and AFM in the middle of LMO layers was inferred from XMLD and XMCD measurements. Polarization-resolved scattering measurements in a magnetic field with π and σ incident light and scattered beam polarization analysis are necessary to separate different magnetic and orbital contributions to scattering at the Mn $L_{3,2}$ edges.

We discuss the O K edge briefly. The measurements at $L = 1$ at the O K edge show that the middle of the SMO (f_S) and LMO (f_L) layers have different doping levels. Oxygen doping is consistent with our observations (Fig. 2), other measurements[24] and certain models[14]. The case of the doped holes in the interface f_i and near-interface f_{ni} layers is different. The interface FM state of this $n = 2$ SL is the metallic state observed in a $n = 4$ SL (Ref. 20). Interface T-dependent states are accessed with scattering at specific momenta L, as determined by the symmetry of the SL structure. The reflection at $L = 1$ (Fig. 2) is not sensitive to T-dependent scattering because, as for the Mn L edges, $\delta S(L = 1) = 0$. The interface states of the $n = 2$ SL of this work are accessed with scattering at $L = 2$ [Eq. (6)], which corresponds to scattering at the $L = 3$ reflection for the $n = 4$ SL in Ref. 20. To determine whether T-dependent scattering occurs at the O K edge in this SL, it would be necessary to measure at $L = 2$. However, the x-ray momentum is insufficient to reach $L = 2$ at the O K edge. Without data at $L = 2$ at the O K edge in support, we did not discuss interface oxygen states.

IV. CONCLUSION

X-ray absorption measurements at the O K edge in a $SrMnO_3/LaMnO_3$ superlattice showed a shoulder, corresponding to holes doped on oxygen sites. The shoulder is aligned with the main resonant peak of soft x-ray scattering from the spatial modulation in the density of doped holes.

A large variation in the Mn $L_{3,2}$ line shapes at $L = 2$, but not at $L = 1$, was observed across the FM transition, pointing to scattering from ferromagnetic interfaces. Comparison to fluorescence yield edge energies for different Mn valences showed the presence of scattering contrast at both Mn^{3+} and Mn^{4+} valences. An x-ray scattering model, which includes double-exchange orbitals in the FM state, explains the observed line broadening at lower temperatures.

Having to rely on measurements of the Mn^{3+} resonances only, different methods to determine the charge disproportionation for bulk AFM orders are controversial, with both small and large charge disproportionation obtained. Our RSXS line shapes, for a SL structure with a large intrinsic charge disproportionation, add an experimental constraint on these competing models.

The development of the SL FM order was accessed with x-ray resonant magnetic scattering and no applied magnetic fields. An open question is the trace [FC or ZFC in Fig. 6(a)] that the height of resonance C would follow on further cooling.

We would like to contrast our measurements to polarized neutron reflectivity (PNR) data on SMO/LMO superlattices (Refs. 38,41), where a magnetic modulation was measured with a period equal to the SL superperiod (magnetization strongly suppressed in SMO, high in LMO). In contrast, the RSXS measurements presented here show an ordering of magnetic moments with a period equal to half the SL superperiod. Several factors may be at the origin of this difference. First, the experimental conditions of the PNR and RSXS measurements were different. Specifically, PNR measurements were made in relatively high fields (0.55 T and 0.82 T in Ref. 38 and 41, respectively), while the RSXS measurements were made with no applied fields. Second, the samples measured in this work have a lower SL superperiod ($n = 2$) compared to the samples of PNR measurements ($n = 3$ and $n = 5$). Thus, a complete mapping of the magnetic structure of SMO/LMO superlattices as a function of deposition se-

quence, magnetic field and temperature requires more measurements.

V. ACKNOWLEDGMENTS

This work was supported by the Department of Energy Office of Basic Energy Science: RSXS measurements by grant DE-FG02-06ER46285, NSLS facilities by DE-AC02-98CH10886, and MRL facilities by DE-FG02-07ER46453 and DE-FG02-07ER46471. Work at Argonne National Laboratory, including use of facilities at the Center for Nanoscale Materials, was supported by the U.S. Department of Energy, Office of Basic Energy Sciences under contract No. DE-AC02-06CH11357.

[1] E.O. Wollan and W.C. Koehler, Phys. Rev. **100**, 545 (1955).
[2] J.B. Goodenough, Phys. Rev. **100**, 564 (1955).
[3] P.-G. de Gennes, Phys. Rev. **118**, 141 (1960).
[4] P.W. Anderson, Phys. Rev. **79**, 350 (1950).
[5] C. Zener, Phys. Rev. **82**, 403 (1951).
[6] P.W. Anderson and H. Hasegawa, Phys. Rev. **100**, 675 (1955).
[7] S. Jin, T.H. Tiefel, M. McCormack, R.A. Fastnacht, R. Ramesh, and L.H. Chen, Science **264**, 413 (1994).
[8] K.J. Thomas, J. P. Hill, S. Grenier, Y-J. Kim, P. Abbamonte, L. Venema, A. Rusydi, Y. Tomioka, Y. Tokura, D.F. McMorrow, G. Sawatzky, and M. van Veenendaal, Phys. Rev. Lett. **92**, 237204 (2004).
[9] S.B. Wilkins, P.D. Spencer, P.D. Hatton, S.P. Collins, M.D. Roper, D. Prabhakaran, and A.T. Boothroyd, Phys. Rev. Lett. **91**, 167205 (2003).
[10] S.S. Dhesi, A. Mirone, C. De Nadai, P. Ohresser, P. Bencok, N.B. Brookes, P. Reutler, A. Revcolevschi, A. Tagliaferri, O. Toulemonde, and G. van der Laan, Phys. Rev. Lett. **92**, 056403 (2004).
[11] S.B. Wilkins, N. Stojic, T.A.W. Beale, N. Binggeli, C.W.M. Castleton, P. Bencok, D. Prabhakaran, A.T. Boothroyd, P.D. Hatton, and M. Altarelli, Phys. Rev. B **71**, 245102 (2005).
[12] S.B. Wilkins, N Stojic, T.A.W. Beale, N. Binggeli, P.D. Hatton, P. Bencok, S. Stanescu, J.F. Mitchell, P. Abbamonte, and M. Altarelli, J. Phys.: Condens. Matter **18**, L323 (2006).
[13] U. Staub, M. Garcia-Fernandez, Y. Bodenthin, V. Scagnoli, R.A. De Souza, M. Garganourakis, E. Pomjakushina, and K. Conder, Phys. Rev. B **79**, 224419 (2009).
[14] M. Garcia-Fernandez, U. Staub, Y. Bodenthin, V. Pomjakushin, A. Mirone, J. Fernandez-Rodriguez, V. Scagnoli, A. M. Mulders, S.M. Lawrence, and E. Pomjakushina, Phys. Rev. B **82**, 235108 (2010).
[15] S.Y. Zhou, Y. Zhu, M.C. Langner, Y.-D. Chuang, P. Yu, W.L. Yang, A.G. Cruz Gonzalez, N. Tahir, M. Rini, Y.-H. Chu, R. Ramesh, D.-H. Lee, Y. Tomioka, Y. Tokura, Z. Hussain, and R.W. Schoenlein, Phys. Rev. Lett. **106**, 186404 (2011).
[16] H. Ehrke, R.I. Tobey, S. Wall, S.A. Cavill, M. Forst, V. Khanna, Th. Garl, N. Stojanovic, D. Prabhakaran, A. T. Boothroyd, M. Gensch, A. Mirone, P. Reutler, A. Revcolevschi, S. S. Dhesi, and A. Cavalleri, Phys. Rev. Lett. **106**, 217401 (2011).
[17] N. Stojic, N. Binggeli, and M. Altarelli, Phys. Rev. B **72**, 104108 (2005).
[18] C.W.M. Castleton and M. Altarelli, Phys. Rev. B **62**, 1033 (2000).
[19] O. Bunau, PhD thesis, University of Grenoble (2010).
[20] S. Smadici, P. Abbamonte, A. Bhattacharya, X. Zhai, B. Jiang, A. Rusydi, J.N. Eckstein, S.D. Bader, and J-M. Zuo, Phys. Rev. Lett. **99**, 196404 (2007).
[21] O. Chmaissem, B. Dabrowski, S. Kolesnik, J. Mais, D.E. Brown, R. Kruk, P. Prior, B. Pyles, and J.D. Jorgensen, Phys. Rev. B **64**, 134412 (2001).
[22] J. Rodriguez-Carvajal, M. Hennion, F. Moussa, A. H. Moudden, L. Pinsard, and A. Revcolevschi, Phys. Rev. B **57**, R3189 (1998).
[23] S. Smadici, J.C.T. Lee, J. Morales, G. Logvenov, O. Pelleg, I. Bozovic, Y. Zhu and P. Abbamonte, Phys. Rev. B **84**, 155411 (2011).
[24] H.L. Ju, H-C. Sohn, and K.M. Krishnan, Phys. Rev. Lett. **79**, 3230 (1997).
[25] S. P. Cramer, F.M.F. deCroot, Y. Ma, C.T. Chen, F. Sette, C.A. Kipke, D.M. Eichhorn, M.K. Chan, W.H. Armstrong, E. Libby, G. Christou, S. Brooker, V. McKee, 0.C. Mullins, and J. C. Fuggle, J. Am. Chem. Soc. **113**, 7937 (1991).
[26] F. Morales, F.M.F. de Groot, P. Glatzel, E. Kleimenov, H. Bluhm, M. Havecker, A. Knop-Gericke, and B.M. Weckhuysen, J. Phys. Chem. B **108**, 16201 (2004).
[27] J. Lee, B. Kim, B.H. Kim, B.I. Min, S. Kolesnik, O. Chmaissem, J. Mais, B. Dabrowski, H.J. Shin, D.H. Kim, H.J. Lee, and J.-S. Kang, Phys. Rev. B **80**, 205112 (2009).
[28] P. Abbamonte, A. Rusydi, S. Smadici, G.D. Gu, G.A. Sawatzky, and D.L. Feng, Nature Physics **1**, 155-158 (2005).
[29] J.-S. Lee, C.-C. Kao, C.S. Nelson, H. Jang, K.-T. Ko, S.B. Kim, Y.J. Choi, S.-W. Cheong, S. Smadici, P. Abbamonte, and J.-H. Park, Phys. Rev. Lett. **107**, 037206 (2011).
[30] S. Smadici, J.C.T. Lee, S. Wang, P. Abbamonte, G. Logvenov, A. Gozar, C. Deville Cavellin, and I. Bozovic, Phys. Rev. Lett. **102**, 107004 (2009).
[31] S. Smadici, J.C.T. Lee, A. Rusydi, G. Logvenov, I. Bozovic, and P. Abbamonte, Phys. Rev. B **85**, 094519 (2012).
[32] C.C. Kao, J.B. Hastings, E.D. Johnson, D.P. Siddons, G.C. Smith, and G.A. Prinz, Phys. Rev. Lett. **65**, 373 (1990).
[33] C.C. Kao, C.T. Chen, E.D. Johnson, J.B. Hastings, H.J. Lin, G.H. Ho, G. Meigs, J.-M. Brot, S.L. Hulbert, Y.U. Idzerda, and C. Vettier, Phys. Rev. B **50**, 9599 (1994).
[34] J.M. Tonnerre, L. Seve, D. Raoux, G. Soullie, B. Rodmacq, and P. Wolfers, Phys. Rev. Lett. **75**, 740 (1995).
[35] M. Abbate, F.M.F. de Groot, J.C. Fuggle, A. Fujimori, O. Strebel, F. Lopez, M. Domke, G. Kaindl, G.A. Sawatzky, M. Takano, Y. Takeda, H. Eisaki, and S. Uchida, Phys. Rev. B **46**, 4511 (1992).
[36] T. Saitoh, A.E. Bocquet, T. Mizokawa, H. Namatame, A. Fujimori, M. Abbate, Y. Takeda, and M. Takano, Phys. Rev. B **51**, 13942 (1995).

[37] J. Topfer and J.B. Goodenough, J. of Solid State Chemistry **130**, 117 (1997).
[38] S.J. May, A.B. Shah, S.G.E. te Velthuis, M.R. Fitzsimmons, J.M. Zuo, X. Zhai, J.N. Eckstein, S.D. Bader, and A. Bhattacharya, Phys. Rev. B **77**, 174409 (2008).
[39] A. Bhattacharya, S.J. May, S.G.E. te Velthuis, M. Warusawithana, X. Zhai, B. Jiang, J.-M. Zuo, M.R. Fitzsimmons, S.D. Bader, and J.N. Eckstein, Phys. Rev. Lett. **100**, 257203 (2008).
[40] B.B. Nelson-Cheeseman *et al.* (unpublished).
[41] T.S. Santos, B.J. Kirby, S. Kumar, S.J. May, J.A. Borchers, B.B. Maranville, J. Zarestky, S.G.E. te Velthuis, J. van den Brink, and A. Bhattacharya, Phys. Rev. Lett. **107**, 167202 (2011).
[42] J.P. Hannon, G.T. Trammell, M. Blume, and D. Gibbs, Phys. Rev. Lett. **61**, 1245 (1988).
[43] F. de Groot, Coordination Chemistry Reviews **249**, 31 (2005).
[44] Z. Hu, G. Kaindl, S.A. Warda, D. Reinen, F.M.F. de Groot, and B.G. Muller, Chemical Physics **232**, 63 (1998).
[45] H.Y. Hwang, S.W. Cheong, P.G. Radaelli, M. Marezio, and B. Batlogg, Phys. Rev. Lett. **75**, 914 (1995).
[46] A.J. Millis, R. Mueller, and B.I. Shraiman, Phys. Rev. B **54**, 5405 (1996).
[47] C. Aruta, C. Adamo, A. Galdi, P. Orgiani, V. Bisogni, N.B. Brookes, J.C. Cezar, P. Thakur, C.A. Perroni, G. De Filippis, V. Cataudella, D.G. Schlom, L. Maritato, and G. Ghiringhelli, Phys. Rev. B **80**, 140405(R) (2009).